


# Development of back side technology for light trapping and photon recycling in GaAs solar cells

Daniel Neves Micha<sup>1,2</sup>  | Oliver Höhn<sup>1</sup> | Eduard Oliva<sup>1</sup> | Vera Klinger<sup>1</sup> |  
Andreas W. Bett<sup>1</sup> | Frank Dimroth<sup>1</sup> 

<sup>1</sup>Fraunhofer Institute for Solar Energy Systems, ISE, Freiburg 79110, Germany

<sup>2</sup>Centro Federal de Educação Tecnológica, CEFET/RJ, Petrópolis 25620-003, Brazil

## Correspondence

Daniel Neves Micha, Centro Federal de Educação Tecnológica, CEFET/RJ, Petrópolis 25620-003, Brazil.

Email: daniel.micha@cefet-rj.br

## Funding information

CNPq-Brasil, Grant/Award Number: 211986/2013-5; ESA, Grant/Award Number: 4000104852

## Abstract

In this work, we propose and realize three different design strategies to implement an optical cavity in GaAs thin film solar cells in order to confine its internal luminescence and hence to exploit photon recycling. The strategies are based on the definition of a highly reflective and very conductive back side, whereas front side light extraction is limited by total internal reflection. We show characterization results on the internal reflectivity of the back reflector and on the contact resistance at the rear side, important quantities for a good functioning of the final solar cell. First, a back side using only metal was optimized with a pure Ag layer leading to an internal reflectivity of 95.2% and a contact resistance of  $1.0 \times 10^{-4} \Omega$  for a  $1 \text{ cm}^2$  device. With a metal-dielectric stack at the back side and electrical contacts made by metals via point-contacts, a second approach led to averaged internal reflectivity of 98.0% and contact resistance of  $1.8 \times 10^{-4} \Omega$  for a  $1 \text{ cm}^2$  device. A third strategy in which a transparent conductive oxide in combination with a metal layer was used did not show the expected results in optical and electrical properties. We fabricated and characterized solar cells with the most promising back sides. When comparing with an ordinary reference GaAs solar cell, external radiative efficiency increased by factors of 150% and 90% for the thin film solar cells with pure Ag and with the metal-dielectric stack at the back side, allowing enhancements of 19 and 13 mV in  $V_{OC}$ , respectively.

## KEYWORDS

back side reflector, GaAs solar cell, open circuit voltage, photon recycling, photovoltaics, thin film solar cell

## 1 | INTRODUCTION

In recent years, the efficiency of single-junction photovoltaic devices for 1-sun applications has been pushed closer to the well-known Shockley-Queisser limit<sup>1</sup> by managing the photon flux within the active regions of solar cells, a concept known as photon management. Radiatively limited solar cells, fabricated out of high quality GaAs<sup>2-5</sup> and GaInP<sup>6</sup> material, benefit from a strong enhancement in open-circuit voltage ( $V_{OC}$ ) if photon recycling effects are exploited. Multi-junction

solar cells can also benefit from photon management through luminescence coupling amongst its junctions and photon recycling effects which would ultimately improve energy conversion efficiency by better current matching conditions and  $V_{OC}$  increase.<sup>7-9</sup> Photon management also brings advantages to nanostructured devices in which several repetitions of active layers of quantum wells or quantum dots are commonly necessary to boost optical properties.<sup>10,11</sup> Furthermore, as a general benefit of photon management, cost of materials can also be reduced. If the incoming sunlight is confined in the active region of

a device, less volume of material is required for absorption. In addition, short circuit current density ( $J_{SC}$ ) can be increased as well as the energy conversion efficiency.<sup>12–14</sup>

The maximum benefit of the photon recycling concept relies on the minimization of the photon flux emitted by the solar cell to its external environment.<sup>8,15–18</sup> Since this flux is omnidirectional, it can be contained within the solar cell active region by limiting the front surface escape cone and reducing the flux transmitted through the rear of the cell. Thus, this light confinement approach increases the photon path length of the luminescence light which effectively reduces the radiative recombination component of the cell's saturation current,<sup>19</sup> increasing  $V_{OC}$ .

From thermodynamic principles,<sup>16</sup> it is possible to correlate  $V_{OC}$  with the external radiative efficiency ( $ERE$ ) of a solar cell through Equation 1:

$$V_{OC} = V_{OC}^{ideal} + \frac{kT}{e} \ln(ERE) \quad (1)$$

in which  $V_{OC}^{ideal}$  is the detailed balance limited  $V_{OC}$  of an ideal solar cell,  $k$  is the Boltzmann constant,  $T$  is the cell temperature, and  $e$  is the elementary charge. From Equation 1, it is possible to conclude that a higher  $ERE$  shifts the solar cell closer to its detailed balance limit for  $V_{OC}$ , which is 1.145 V for a GaAs device. On the other hand,  $ERE$  can be calculated by the solar cell figures of merit and its spectral external quantum efficiency ( $EQE$ ), as in Equation 2.<sup>20</sup>

$$ERE = \frac{2\pi e}{h^3 c^2} \left( \frac{1}{J_{SC}} \right) \cdot \exp\left(\frac{eV_{OC}}{kT}\right) \cdot \int_{E_g}^{\infty} \frac{\overline{EQE} \cdot E^2}{\exp(E/kT) - 1} dE \quad (2)$$

In Equation 2,  $h$  denotes the Planck constant,  $c$  the speed of light,  $E_g$  the active material bandgap energy, and  $\overline{EQE}$  is the weighted value of  $EQE$  over all angles of incident light. According to Green,<sup>20</sup> this can be well approximated to its perpendicular value for a high-quality device.

Figure 1 shows the timeline for the figures of merit of GaAs thin film solar cells ( $TFSC$ ) from 1993 to 2018. It is remarkable that  $V_{OC}$  has been the most important factor in the raise of efficiency over the last years. In the same way, GaAs solar cells'  $ERE$  has followed the rapid historical increase of  $V_{OC}$  going from 1.1% in 2005 and 1.7% in 2009 with the devices fabricated by the Radboud University group to 22.5% in 2011 and 54% in 2012 achieved with the  $TFSC$  of Alta Devices Inc. (according to Equation 2 applied to data from Green

et al and Bauhuis et al,<sup>21,22,28,29</sup> respectively). Along with a better material quality, a photon management method, such as the use of very reflective back side reflectors, has also been implemented to realize such improvement in  $ERE$ . In comparison, the best reported GaAs solar cell without any photon management reached a  $V_{OC}$  of 1030 mV and an  $ERE$  of 1.26%.<sup>20</sup> For other devices'  $ERE$  and further discussions, please see Green.<sup>20</sup>

The main objective of this paper is to show experimental results on different technological design strategies to implement a very reflective and conductive back side in GaAs  $TFSC$ . First, the strategies are described in Section 2. In Section 3, the samples designed to investigate the electrical and optical properties of the back side technology are described as well as the characterization results. Section 4 is dedicated to a description of the solar cells fabrication with the best back side technologies described in the previous sections. The characterization results of such devices and discussions follow in Section 5, and the conclusions are given in Section 6.

## 2 | OPTICAL AND ELECTRICAL DESIGN STRATEGIES TO THE BACK SIDE OF SOLAR CELLS

A significant number of proposals have been made in literature on how to form an optical cavity in which photons are confined to the active region of a solar cell. This includes the design of the back and the front sides of the device. For the back side, metallic mirrors, diffraction gratings, photonic structures, and others<sup>7,29–33</sup> have been tested to reflect and/or diffuse the photon flux to be recycled back to the active region of the cell. For any of these approaches, the formation of a good reflector/diffusor must be conciliated with the preservation of a good electrical contact. For the front side, light directors, photonic and plasmonic structures<sup>34–38</sup> were proposed to manage the outgoing light. Here, the trade-off is between the benefits brought to the device by light management and the shadowing losses.

In this work, the formation of an optical cavity in GaAs  $TFSC$  is based on a planar back side reflector at the rear side and on the natural limited cone ( $\theta_C \approx 16^\circ$ ) for total internal reflection of the front side semiconductor/ARC/air interface, as shown in Figure 2.

In order to achieve a high reflectivity and high electrical conductivity, three different design strategies for the back side of the device were proposed and tested according to Figure 3: (A) a full area stack of

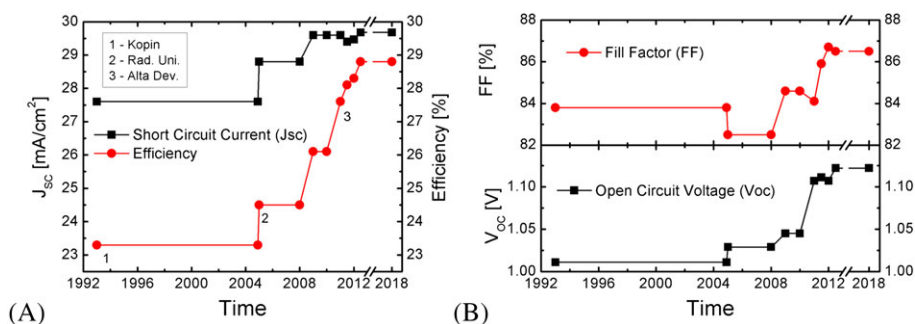


**FIGURE 1** Timeline of the performance metrics of GaAs thin film solar cells<sup>21–27</sup>: A, efficiency and  $J_{SC}$ ; and B, FF and  $V_{OC}$  [Colour figure can be viewed at [wileyonlinelibrary.com](http://wileyonlinelibrary.com)]

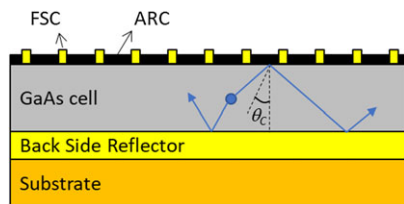


**FIGURE 2** Optical design for the back and the front side of a GaAs thin film solar cell in order to create a cavity around the active layers. FSC and ARC are abbreviations for front side contact and anti-reflective coating, respectively [Colour figure can be viewed at [wileyonlinelibrary.com](http://wileyonlinelibrary.com)]

metal layers; (B) a full area transparent conductive oxide layer followed by a full area metal layer; and (C) a metal-dielectric stack with point-contacts. It is important to note that the substrate indicated in Figures 2 and 3 is not the original substrate used for growth but any one defined during processing (after growth) to mechanically support the devices and conduct the electrical current. In our case, the substrates were defined by electroplating, as will be described in Section 4.

Strategy (A) is based on the natural high reflectivity and high electrical conductivity of metals.<sup>13,28,29</sup> Here, the challenge is to find an appropriate selection of low absorptive metals that make a good ohmic contact to the adjacent semiconductor layer without the need of high annealing temperatures which would cause diffusion and would smear out the joint interface. Strategy (B) relies on the low refractive index and on the electrical conductivity of a transparent conductive oxide.<sup>39,40</sup> Photons transmitted through the high reflective interface between the oxide and the semiconductor would have a second chance of getting reflected at the metal surface. However, to increase the electrical conductivity of the transparent conductive oxide, it is necessary to increase the oxide doping which changes its transparency.<sup>41,42</sup> This imposes a trade-off between electrical and optical properties. Finally, strategy (C) joins ideas of the two previous approaches. Instead of a conductive oxide, as used in (B), a stack composed of a highly transparent dielectric layer with low refractive index followed by a highly reflective metal is deposited on the semiconductor.<sup>12,13</sup> Afterwards, holes are opened in the dielectric by photolithography in which a metal (or stack of metals) is deposited, defining electrical point contacts. In this way, it is possible to choose the proper metals to form an ohmic contact to the semiconductor independently of the metal (s) used for reflection. In this approach, the trade-off is between the balancing of the areas for reflection and electrical conduction.

### 3 | REALIZATION AND CHARACTERIZATION OF THE BACK SIDE TECHNOLOGIES

Test samples were designed and grown by metal organic vapor phase epitaxy for electrical and optical tests of the back side technology prior to the final application in the solar cells.

The structure of the samples used for electrical conductivity tests is composed of a 1000-nm highly doped ( $5 \times 10^{19} \text{ cm}^{-3}$ )  $\text{Al}_{0.10}\text{Ga}_{0.90}\text{As}$  layer on top of a GaAs buffer layer. The Al content in the alloy was chosen to avoid any parasitic absorption of the luminescence coming from the active layer. The high doping level improves the sheet resistance and the resistivity of the back side contact. Transmission line method<sup>43</sup> structures were manufactured to determine the contact resistivity of the metals and/or transparent conductive oxides deposited on the epitaxy films.

The reflectivity of the back side technology cannot be measured directly in a structure similar to the final device, as the active material (GaAs) would absorb the light in the wavelength range of interest (800–900 nm). So, a material with a bandgap energy higher than GaAs was chosen to investigate the reflection. It is still important that this material has a refractive index close to GaAs so that the reflectivity being measured is very close to the real situation in the final devices. The alloy  $\text{Ga}_{0.50}\text{In}_{0.50}\text{P}$ , which is lattice matched to GaAs and has a cutoff wavelength of 670 nm and an average refractive index of 3.27 (10% lower than GaAs), was selected.

The samples used to investigate reflectivity have the structure depicted in Figure 4A. Several steps are taken to fabricate such a structure as follows according to the sequence in Figure 4B: (I) growth, (II) deposition of the materials used as back side reflector on top of the GaInP layer followed by attachment of the resulting structure to a mechanical holder by gluing, and (III) removal of the substrate and the etching stopping layers by chemical wet etching.

The GaInP surface is treated with a solution of ammonium hydroxide immediately before the deposition of the back side reflector to remove native oxides. The substrate is removed by selective wet etching with a solution of  $\text{NH}_4\text{OH}/\text{H}_2\text{O}_2$  at 60°C. Finally, the removal of the GaInP and GaAs etching stopping layers is also done with selective wet etching with HCl at room temperature, and with a solution of citric acid/ $\text{H}_2\text{O}/\text{H}_2\text{O}_2$  at room temperature, respectively.

Reflectivity measurements were performed in a Cary 500i taking a white standard as reference. In the experiment, light from a broad band source impinges almost perpendicular to the test sample (with an angle less than 2°) undergoes multiple reflection in an integrating sphere until it is collected by a Si detector. By using a procedure involving the transfer matrix method<sup>44</sup> applied to the

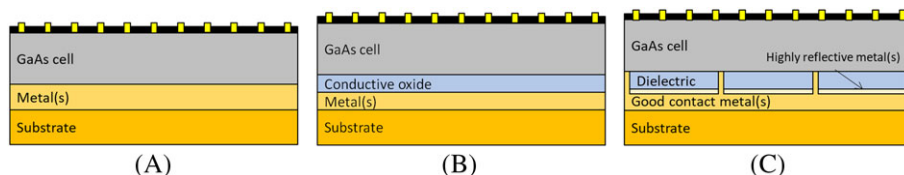


**FIGURE 3** Schematic representation of three design strategies for the back side technology of GaAs solar cells: A, a stack of metals; B, a stack of transparent conductive oxide and metals; and C, a metal-dielectric stack [Colour figure can be viewed at [wileyonlinelibrary.com](http://wileyonlinelibrary.com)]

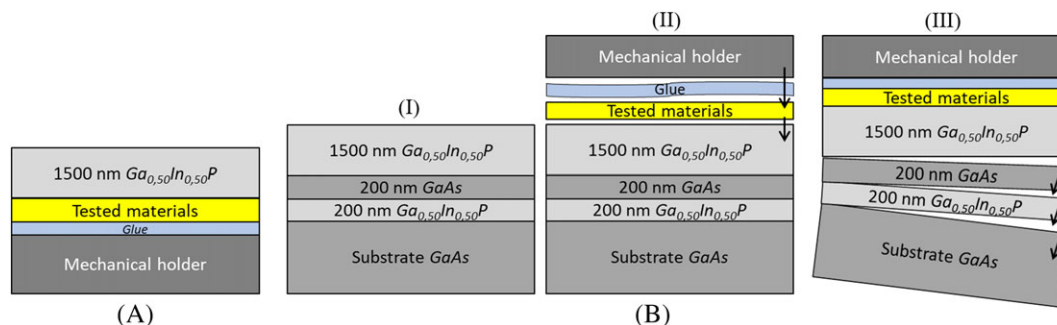


**FIGURE 4** A, Layer structure of the test sample used to probe optical reflectivity of the back side technologies. In (B), the fabrication steps are shown [Colour figure can be viewed at [wileyonlinelibrary.com](http://wileyonlinelibrary.com)]

multilayered structures of the test samples, the reflectivity spectrum ( $R_i$ ) of the internal GaInP/reflector interface can be extracted. The transfer matrix method code used (*TMTTool*) was developed at Fraunhofer ISE and is implemented in such a way to take into consideration the  $n$ - $k$  (refractive index-extinction coefficient) data for all the materials used in the stacks. In this way, not only reflection of each interface given by Fresnel laws is considered but absorption in the materials as well.

Figure 5 illustrates the procedure mentioned above for a double layer of Ti/Au: 1/150 nm used as back side reflector. Firstly, the experimental external reflectivity data (black squares) are compared with the simulated reflectivity spectrum (red dot-dashed curve) obtained by *TMTTool* using the same nominal growth structure (inset "a") and optical data from various literature sources.<sup>45</sup> As can be seen in the figure, the theoretical result deviates from the experimental data. Then, the layer thicknesses are optimized through trial and error until the theoretical reflectivity shows a better agreement with the experimental data. In this case, this occurred with a thickness of 1550 nm for the GaInP and 4 nm for the Ti layer. With the effective structure defined, the incident medium is changed from air to GaInP (inset "b") in the simulations in order to obtain the internal reflectivity spectrum (blue dashed curve).

Table 1 presents results on optical–internal reflectivity averaged between 800 and 900 nm ( $R_i$ )—and electrical—contact resistivity  $\rho_c$ —properties of some material combinations tested as back side reflector

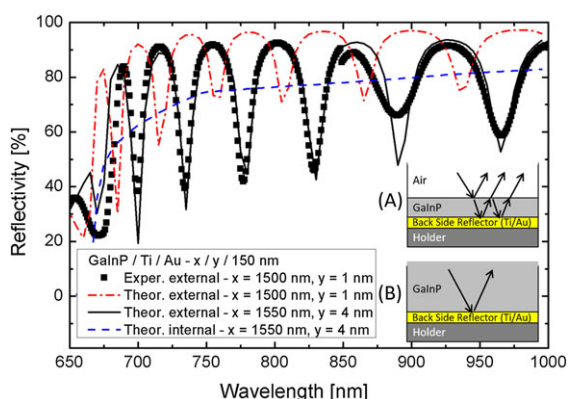


**FIGURE 5** Representation of the procedure used to extract the internal reflectivity of the back side reflector, in this case a double layer of Ti/Au. The insets show the structures used in the simulation to extract A, the external reflectivity and B, the internal reflectivity [Colour figure can be viewed at [wileyonlinelibrary.com](http://wileyonlinelibrary.com)]

for the three design strategies previously described. Two different methods of material deposition were used: (1)—thermal evaporation, and (2)—sputtering. For some material combinations, such as dielectrics and metals, it was necessary to combine both methods in sequence because evaporation did not assure enough adhesion of the stack to the semiconductor, as verified by tape tests. The results reported in the table are for structures in which no high temperature steps were taken to alloy the metals, as such processes showed to degrade the optical performance. Electrical tests were done in which the ohmic behavior was observed even without an annealing process for all contacts shown in the table.

As an obvious choice of material for the back side reflector due to its well-known high reflectivity, pure Au was one of the tested metals for strategy (A). However, due to insufficient adhesion, it was not possible to characterize the optical and electrical properties of such a sample. This is the reason why a very thin adhesion promoter layer of Ti was included which unfortunately lowers the reflectivity. The insertion of Pd in between the two metals was to improve electrical properties, which indeed happened as can be seen in Table 1. But the optical properties were found to degrade with increasing thickness of the Pd layer. For design strategy (A), only pure Ag showed the required optical property to be used as a good back side reflector. Pd/Zn/Pd/Au is shown in the table because it is a standard metal stack for p-type GaAs. Its reflectivity is not high enough for application as design strategy (A) but is a good choice for the electrical contact in strategy (C). Aluminum-doped zinc oxide (AZO) was the transparent conductive oxide used for design strategy (B). The experimental results differ strongly from the simulated internal reflectivity, which was around 97%. We attribute this to the roughening of the AZO/semiconductor interface by the sputtering technique. Furthermore, it has been already shown in literature that plasmonic absorption is detrimental to the reflectivity of AZO/Ag in the relevant wavelength range,<sup>46</sup> which can also partially explain our result. Along with that, electrical resistivity was very poor. A more thorough study concerning the doping level and the thickness of the oxide layer as well as the surface preparation may still be necessary to draw a complete conclusion for this design strategy. Finally, materials tested for strategy (C) showed very promising results. Reflectivity higher than 98% was obtained for all metal-dielectric stack combinations. Here, AZO was used as adherent material between dielectrics and Ag.

With Pd/Zn/Pd/Au as electrical contact covering around 1% of the total area for design strategy (C), the resistance of the back

**TABLE 1** Optical and electrical characterization results of the material combinations tested in the three strategies designed for the back side technology of GaAs TFSC. The deposition methods were 1—evaporation and 2—sputtering

Design Strategy	Materials	Thickness, nm	Deposition Method	$\langle R_i \rangle$ , %	$\rho_c$ , $10^{-4} \Omega \text{cm}^2$
(a)	Ti/Au	1/150	1	79.8	$3.26 \pm 0.04$
(a)	Ti/Pd/Au	1/20/150	1	48.0	$2.250 \pm 0.002$
(a)	Ti/Pd/Au	1/40/150	1	46.5	$2.37 \pm 0.02$
(a/c)	Pd/Zn/Pd/Au	20/20/30/200	1	30.0	0.018
(a)	Ag	150	1	95.2	$0.9 \pm 0.1$
(b)	AZO/Ag	20/150	2	85.0	$\sim 100$
(b)	AZO/Ag	90/150	2	85.0	$\sim 100$
(c)	MgF <sub>2</sub> */AZO**/Ag**	120/20/150	*1/**2	98.6	-
(c)	SiO <sub>2</sub> */AZO**/Ag**	120/20/150	*1/**2	98.6	-
(c)	Al <sub>2</sub> O <sub>3</sub> */AZO**/Ag**	90/20/150	*1/**2	98.6	-

contact is  $1.8 \times 10^{-4} \Omega$  for a  $1\text{-cm}^2$  device which is similar to the ones using design strategy (A) of  $1.0 \times 10^{-4} \Omega$  for a device with the same area. At the same time, area for reflectivity is 99% of total area in such a way to decrease the averaged reflectivity to 98.0%.

By finding proper materials for the back side technology, we decided to follow on in the fabrication of the solar cells with design strategy (A) using pure Ag as back side reflector and electrical contact and with design strategy (C) using MgF<sub>2</sub>/AZO/Ag as back side reflector and Pd/Zn/Pd/Au as electrical contact.

#### 4 | SOLAR CELL STRUCTURE AND DEVICES FABRICATION

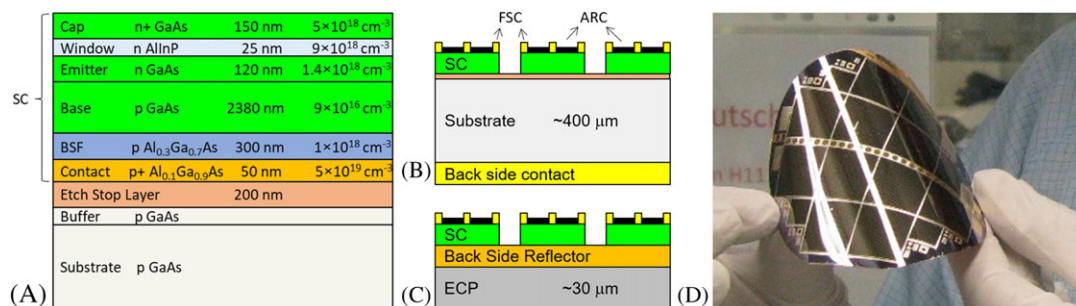
GaAs solar cells were grown by metal organic vapor phase epitaxy on GaAs p-type doped substrates according to the structure depicted in Figure 6A. The active region of the devices is composed of an ordinary structure of layers, such as cap, window, emitter, base, and back surface field whose thicknesses and doping levels are detailed in the figure.

Two different processes were applied to the materials in order to generate the reference solar cell on the original substrate without a back reflector (Figure 6B), hereafter named REFSC, and test solar cells with a reflector defined in between a substrate and the active region (Figure 6C), hereafter named TESTSC (x) in which x is for the used design strategy. The front side processing of all devices follows the same sequence of steps of photolithography, wet etching, and

metallization to define mesa structures of 1 and  $4\text{ cm}^2$  with a metal grid of fingers in the front side contact covering 1.95% of the total area and an MgF<sub>2</sub>/Ta<sub>2</sub>O<sub>5</sub> anti-reflective coating in the complementary area. The back side of the REFSC was coated with a stack of Pd/Zn/Pd/Au which after a thermal annealing defines a low resistance ohmic contact to the GaAs substrate. To process the back side of the TESTSC (x), the steps were as follow: (1) the wafer was temporary attached by the front side to a sapphire holder by gluing, then (2) the original substrate and the (3) Etch Stop layer were chemically removed. With the back side of the solar cells exposed, (4) the materials for the back side reflector/electrical contact were deposited (different in each strategy), and (5) a new copper-based substrate (ECP) was electroplated at the rear side of the devices for mechanical support and electrical contact. Figure 6D shows a full 4" wafer processed under the aforementioned sequence of steps. As the Cu substrate is very thin ( $\approx 30\text{ }\mu\text{m}$ ), the entire foil is flexible and lightweight. While a fully processed wafer with cells on original substrate weights around 19 g, wafer with test cells weighs only 2.0 g, almost 10 times lighter.

#### 5 | SOLAR CELL CHARACTERIZATION

To certify that the effectiveness of the back side reflector holds at device level, reflectivity measurements from the REFSC and the test solar cells were taken in the same setup described in Section 3 used for measuring the GaInP test samples reflectivity. Reflectivity curves are represented as lines in Figure 7. EQE curves, represented by

**FIGURE 6** Schematics of A, materials, thicknesses, and doping levels of solar cell layers, B, device structure of reference solar cell, and C, device structure of test solar cells. In D, a photograph of a 4" GaAs wafer fully processed as 1 and  $4\text{ cm}^2$  thin film solar cells is shown [Colour figure can be viewed at [wileyonlinelibrary.com](http://wileyonlinelibrary.com)]



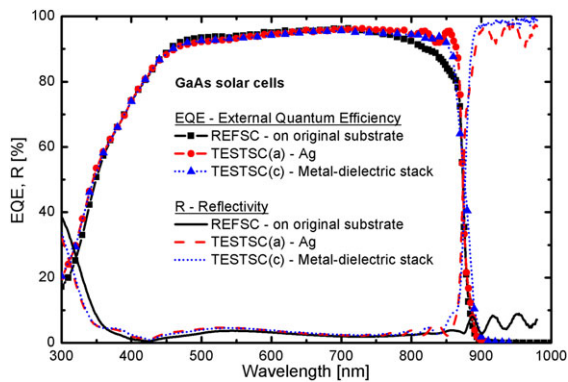


**FIGURE 7** External quantum efficiency (EQE) and external frontal reflectivity (R) of the solar cells [Colour figure can be viewed at [wileyonlinelibrary.com](http://wileyonlinelibrary.com)]

symbols in the same figure, were taken under 25°C and short circuit conditions.

In the wavelength range of 300 to 850 nm, reflectivity is very low for all devices due to the inhibition of reflection by the anti-reflective coating and absorption by the active material—GaAs. For longer wavelengths, reflectivity stays low for the REFSC but is very high for both TESTSC (A) and TESTSC (C), indicating the effectiveness of the back side reflector and confirming the results previously obtained from the test samples.

Current density-voltage (JV) measurements were taken with a solar simulator setup under standard test conditions, namely AM1.5 g spectrum and 25°C. Table 2 summarizes the figures of merit extracted from such curves.

From the longer wavelength range of experimental EQE, it is possible to understand the increase of as high as 1.4% in  $J_{SC}$  for TESTSC (A) and TESTSC (C) in comparison to the REFSC, as shown in Table 2. Besides reflecting the luminescence light back to the solar cell, the back side reflector also serves to enlarge the sunlight path inside the device giving more chances to solar photons with energy close to the bandgap to be absorbed.

The most important result to highlight though is the large boost in  $V_{OC}$  from 1056 mV for the REFSC to 1069 mV for the TESTSC (C) with metal-dielectric stack as back side reflector and to 1075 mV for the TESTSC (A) with Ag as back side reflector. These gains are expected to come from a better exploitation of photon recycling effect due to the confinement of the luminescence light in the active region of the solar cell. As discussed in Section 1, it is possible to correlate such voltage improvements to enhancements in ERE. Table 3 shows the calculated value of ERE using Equation 2 for all solar cells obtained from JV parameters and EQE spectral data. It is also shown the difference in  $V_{OC}$  in relation to the REFSC from experimental JV curves ( $\delta V_{OC}^{JV}$ ) and the expected difference from Equation 1 ( $\delta V_{OC}^{ERE}$ ) in which a good agreement is obtained. Here, it is important to

**TABLE 2** Figures of merit of the solar cells extracted from JV curves

Solar Cell	$V_{OC}$ , mV	$J_{SC}$ , mA/cm <sup>2</sup>	FF, %	Efficiency, %
REFSC	1056	29.23	82.16	25.35
TESTSC (a)	1075	29.57	79.95	25.41
TESTSC (c)	1069	29.65	80.47	25.51

**TABLE 3** Photon recycling related parameters of the solar cells

Solar Cell	ERE, %	$\delta V_{OC}^{JV}$ , mV	$\delta V_{OC}^{ERE}$ , mV
REFSC	2.99	-	-
TESTSC (a)	7.29	19	23
TESTSC (c)	5.67	13	17

differentiate the gain in  $V_{OC}$  brought by photon recycling effects in the test samples in contrast to the one brought by the pure increase of the  $J_{SC}$  (and the whole curve) due to a large sunlight path, which is estimated to be less than 1 mV.

The higher ERE obtained in this study, 7.29% with TESTSC (A), is still lower than the highest one reached by Alta Devices but can be considered high in comparison to the other TFSC mentioned in Section 1. Furthermore, even the ERE obtained for REFSC, namely 2.99%, is very high in comparison with other solar cells fabricated using a similar technology.

Finally, although FF systematically decreased, the final values for conversion efficiency for both test solar cells increased, despite very slightly.

## 6 | CONCLUSIONS

Three different design strategies for a back side reflector used to define an optical cavity in GaAs TFSCs were reported. Test samples were planned and realized to investigate optical and electrical properties of several different material combinations. Higher reflectivities and lower contact resistances were achieved with two of the three design strategies: with a planar Ag layer that serves simultaneously as back side reflector and electrical back contact, and with a metal-dielectric stack of MgF<sub>2</sub>/AZO/Ag as back side reflector, with electrical point contacts defined by a stack of Pd/Zn/Pd/Au in 1% of the total area. The most successful design strategies presented an internal averaged reflectivity of 95.2% and 98.0% and a contact resistance of  $1.0 \times 10^{-4} \Omega$  and  $1.8 \times 10^{-4} \Omega$  for a 1 cm<sup>2</sup> device, respectively.

GaAs TFSCs were fabricated and characterized with the best technology. The very reflective back side allows for the exploitation of photon recycling. Indeed, the TFSC with planar Ag as back side finishing has shown an ERE of 7.29%, 2.5 times larger than for the reference solar cell on a bulk GaAs substrate. The high radiative efficiency leads to an increase of  $V_{OC}$  of 19 mV from 1056 to 1075 mV, exceeding the logarithmical increase of 1 mV expected from the shift of the JV curve due to a higher  $J_{SC}$ .

The fabricated TFSCs are flexible and almost 10 times lighter than the reference solar cells kept on its original absorptive substrate. Furthermore, they have shown higher efficiencies of up to 25.5% against 25.4% for the reference under the 1-sun AM1.5 g spectrum. By aggregating other technologies, such as epitaxial lift-off, to the ones described here, GaAs TFSCs can become more economically competitive. Besides the costs and the final energy price, applications of this kind of cell in which flexibility and lightness are necessary can be benefited. The power to mass density for 1-sun AM1.5 g is around 1.0 W/g whereas the projected value for AM0 is around 1.2 W/g,

even higher than the standard triple-junction solar cell for space applications.

## ACKNOWLEDGEMENTS

This work was supported by ESA through the project "optimization of photon density in ultra-thin GaAs solar cells" (ESTEC/contract no. 4000104852). The authors would like to thank the Fraunhofer ISE III-V technology team in supporting the processing of the devices, Thomas Kroyer for sputtering depositions, Sandra Bau and Isabella Straub for the electroplating, Simon Barke, Gerard Siefer, and the Fraunhofer ISE III-V Metal Organic Vapor Phase Epitaxy and characterization team for discussions, as well as Elisabeth Schaefer for EQE measurements and the Callab team for JV measurements. Daniel Micha acknowledges the funding from CNPq-Brasil through the project Ciência sem Fronteiras (211986/2013-5).

## ORCID

Daniel Neves Micha  <http://orcid.org/0000-0003-0572-7367>

Frank Dimroth  <http://orcid.org/0000-0002-3615-4437>

## REFERENCES

- Shockley W, Queisser H. Detailed balance limit of efficiency of pn junction solar cells. *Applied Physics Letters*. 1961;32:510-519.
- Steiner MA. Optical enhancement of the open circuit voltage in high quality GaAs solar cells. *Journal of Applied Physics*. 2013;113:123109.
- Walker AW, Höhn O, Micha DN, Bläsi B, Bett AW, Dimroth F. Impact of photon recycling on GaAs solar cell designs. *Journal of Photovoltaics*. 2015;5:1636-1645.
- Schiling CL, Höhn O, Micha DN, et al. Combining photon recycling and concentrated illumination in a GaAs heterojunction solar cell. *Journal of Photovoltaics*. 2018;8:348-354.
- Kayes BM, Nie H, Twist R, Spruytte SG, Reinhardt F, Kizilyalli IC, et al. 27.6% conversion efficiency, a new record for single-junction solar cells under 1 sun illumination. *Proceedings of 37th IEEE Photovoltaic Specialist Conference*. Seattle, June 2011.
- Geisz JF, Steiner MA, García I, Kurtz SR, Friedman DJ. Enhanced external radiative efficiency for 20.8% efficient single-junction GaInP solar cells. *Applied Physics Letters*. 2013;103:1-5.
- Friedman DJ, Geisz JF, Steiner MA. Analysis of multijunction solar cell current-voltage characteristics in the presence of luminescent coupling. *Journal of Photovoltaics*. 2013;3:1429-1436.
- Steiner MA, Geisz JF, Garcia I, et al. Effects of internal luminescence and internal optics on Voc and Jsc of III-V solar cells. *Journal of Photovoltaics*. 2013;3(4):1437-1442.
- Walker AW, Höhn O, Micha DN, et al. Impact of photon recycling and luminescence coupling on III-V single and dual junction photovoltaic devices. *Journal of Photonics for Energy*. 2015;5(1):53087.
- Toprasertpong K, Fujii H, Thomas T, et al. Absorption threshold extended to 1.15 eV using InGaAs/GaAsP quantum wells for over-50%-efficient lattice-matched quad-junction solar cells. *Progress in Photovoltaics: Research and Applications*. 2015;24:533-542.
- Bailey C, Forbes DV, Polly SJ, et al. Open-circuit voltage improvement of InAs/GaAs quantum-dot solar cells using reduced InAs coverage. *Journal of Photovoltaics*. 2012;2(3):269-275.
- Holman ZC, Descoeudres A, De Wolf S, Ballif C. Record infrared internal quantum efficiency in silicon heterojunction solar cells with dielectric/metal rear reflectors. *Journal of Photovoltaics*. 2013;3:1243-1249.
- Cui H, Campbell PR, Green MA. Optimisation of the back surface reflector for textured polycrystalline Si thin film solar cells. *Energy Procedia*. 2013;33:118-128.
- Zhao J, Wang A, Green MA, Ferraza F. 19.8% efficient "honeycomb" textured multicrystalline and 24.4% monocrystalline silicon solar cells. *Applied Physics Letters*. 1995;73:1991-1993.
- Yablonovitch E. Inhibited spontaneous emission in solid-state physics and electronics. *Physical Review Letters*. 1987;58:2059-2062.
- Miller OW, Yablonovitch E, Kurtz SR. Strong internal and external luminescence as solar cells approach the Shockley-Queisser limit. *Journal of Photovoltaics*. 2012;2:303-311.
- Létay G, Hermle M, Bett AW. Simulating single-junction GaAs solar cells including photon recycling. *Progress in Photovoltaics: Research and Applications*. 2006;14:683-696.
- Wang X, Khan MR, Gray JL, Alam MA, Lundstrom MS. Design of GaAs solar cells operating close to the Shockley-Queisser limit. *Journal of Photovoltaics*. 2013;3:737-744.
- Martí A, Balenzategui JL, Reyna RF. Photon recycling and Shockley's diode equation. *Journal of Applied Physics*. 1997;82:4067-4075.
- Green MA. Radiative efficiency of state-of-the-art photovoltaic cells. *Progress in Photovoltaics: Research and Applications*. 2012;20:472-476.
- Green MA, Emery K, Hishikawa Y, Warta W. Solar cell efficiency tables (version 37). *Progress in Photovoltaics: Research and Applications*. 2011;19:84-92.
- Green MA, Emery K, Hishikawa Y, Warta W, Dunlop ED. Solar cell efficiency tables (version 40). *Progress in Photovoltaics: Research and Applications*. 2012;20:606-614.
- Green MA, Emery K. Solar cell efficiency tables (version 2). *Progress in Photovoltaics: Research and Application*. 1993;1:225-227.
- Green MA, Emery K, Hishikawa Y, Warta W. Solar cell efficiency tables (version 32). *Progress in Photovoltaics: Research and Applications*. 2008;16:435-440.
- Green MA, Emery K, Hishikawa Y, Warta W. Solar cell efficiency tables (version 33). *Progress in Photovoltaics: Research and Applications*. 2009;17:85-94.
- Green MA, Emery K, Hishikawa Y, Warta W. Solar cell efficiency tables (version 36). *Progress in Photovoltaics: Research and Applications*. 2010;18:346-352.
- Green MA, Emery K, Hishikawa Y, Warta W, Dunlop ED. Solar cell efficiency tables (version 39). *Progress in Photovoltaics: Research and Applications*. 2012;20:12-20.
- Bauhuis GJ, Mulder P, Schermer JJ, Haverkamp EJ, van Deelen J, Larsen PK. High efficiency thin film GaAs solar cells with improved radiation hardness. In *Proceeding of the 20th European Photovoltaic Solar Energy Conference*, Barcelona, June 2005.
- Bauhuis GJ, Mulder P, Haverkamp EJ, Schermer JJ, Huijben JC. 26.1% thin-film GaAs solar cell using epitaxial lift-off. *Solar Energy Materials and Solar Cells*. 2009;93:1488-1491.
- Atwater HA, Polman A. Plasmonics for improved photovoltaic devices. *Nature Materials*. 2010;9:865.
- Zeng L, Bermel P, Yi Y, et al. Demonstration of enhanced absorption in thin film Si solar cells with textured photonic crystal back reflector. *Applied Physics Letters*. 2008;93(22):221105.
- Zeng L et al. Efficiency enhancement in Si solar cells by textured photonic crystal back reflector. *Applied Physics Letters*. 89:2006, 111111.
- Zhou D, Biswas R. Photonic crystal enhanced light-trapping in thin film solar cells. *Journal of Applied Physics*. 2008;103:093102.
- Schuler JA. Plasmonics for extreme light concentration and manipulation. *Nature Materials*. 2010;9:193-204.
- Polman A, Atwater HA. Photonic design principles for ultrahigh-efficiency photovoltaics. *Nature Materials*. 2012;11:174-177.
- Bermel P, Luo C, Zeng L, Kimerling LC, Joannopoulos J. Improving thin-film crystalline silicon solar cell efficiencies with photonic crystals. *Optics Express*. 2007;15:16986-17000.

37. Peters M, Goldschmidt JC, Blasi B. Efficiency limit and example of a photonic solar cell. *Journal of Applied Physics*. 2011;110:043104.
38. Kosten ED, Kayes BM, Atwater HA. Experimental demonstration of enhanced photon recycling in angle-restricted GaAs solar cells. *Energy & Environmental Science*. 2014;7:1907-1912.
39. Rayerfrancis A, Bhargav PB, Ahmed N, Bhattacharya S, Chandra B, Dhara S. Sputtered AZO thin films for TCO and back reflector applications in improving the efficiency of thin film a-Si:H solar cells. *Silicon*. 2017;9:31-38.
40. Yue G, Sivec L, Owens JM, Yan B, Yang J, Guha S. Optimization of back reflector for high efficiency hydrogenated nanocrystalline silicon solar cells. *Applied Physics Letters*. 2010;95:263501.
41. Qiu Y, Hermawan H, Gordon I, Poortmans J. Direct current sputtered aluminum-doped zinc oxide films for thin crystalline silicon heterojunction solar cell. *Materials Chemistry and Physics*. 2013;141: 744-751.
42. Hamelmann FU. Transparent conductive oxides in thin film photovoltaics. *Journal of Physics: Conference Series*. 2014;559:12016.
43. Reeves GK, Harrison HB. Obtaining the specific contact resistance from transmission line model measurements. *IEEE Electron Device Letters*. 1982;EDL-3:111-113.
44. Macleod HA. *Thin-Film Optical Filters*. 4th ed. Boca Raton, FL: CRC Press; 2010.
45. Palik ED. *Handbook of optical constants of solids*. Orlando: Academic Press; 1985. <https://refractiveindex.info/> (accessed August 12, 2018).
46. Haug FJ, Soderstrom T, Cubero O, Terrazoni-Daudrix V, Ballif C. Plasmonic absorption in textured silver back reflectors of thin film solar cells. *Journal of Applied Physics*. 2008;104:64509.

**How to cite this article:** Micha DN, Höhn O, Oliva E, Klinger V, Bett AW, Dimroth F. Development of back side technology for light trapping and photon recycling in GaAs solar cells. *Prog Photovolt Res Appl*. 2018;1-8. <https://doi.org/10.1002/pip.3076>